JOM, Vol. 74, No. 3, 2022
https://doi.org/10.1007/s11837-021-05033-x

The Anisotropic Yield Surface of Cellular Materials

KAITLYNN M. CONWAY,[1] ZACHARY ROMANICK,[1] LEA M. COOK,[1] LUIS A. MORALES,[1] JONATHAN D. DESPEAUX,[1] MARCUS L. RIDLEHUBER,[1] CHRISTIAN FINGAR,[1] DAQUAN DOCTOR,[1] CHETAN P. NIKHARE,[2] and GARRETT J. PATAKY[1,3]

1.—Department of Mechanical Engineering, Clemson University, Clemson, SC 29634, USA. 2.—Department of Mechanical Engineering, The Pennsylvania State University Erie, Erie, PA 16563, USA. 3.—e-mail: gpataky@clemson.edu

The use of mechanical metamaterials in engineering applications is often limited because of uncertainty regarding their deformation behavior. This uncertainty necessitates large safety factors and assumptions about their behavior to be included in mechanical designs including metamaterials, which detracts from their greatest benefit, viz. their ultralight weight. In this study, a yield envelope was created for both a bending-dominated and a stretching-dominated cellular material topology to improve the understanding of the response of cellular materials under various load types and orientations. Experimental studies revealed that the shear strength of a cellular material is significantly lower than that predicted by Mohr's criterion, necessitating a modification of the Mohr's yield criterion for cellular materials. All topologies experienced tension–compression anisotropy and topology orientation anisotropy during loading, with the stretching-dominated topology experiencing the largest anisotropies.

INTRODUCTION

In terms of specific strength, monolithic materials are limited by their elemental weights, creating a ceiling of what can be achieved using solid materials alone. An increasingly popular method for manipulating a material's properties is by adjusting the geometric arrangement or topology of the material's mesostructure.[1] Low-density metamaterials combine solid materials and zero-density voids to occupy material property spaces that are not achievable using monolithic materials.[2] The complex geometric freedoms of additive manufacturing (AM) enable the creation of metamaterial topologies with significantly altered mechanical properties compared with the base materials.[3] However, understanding of the mechanics responsible for the deformation behavior of such metamaterials, particularly their fracture and failure, across different environments and loading situations is limited, necessitating large safety factors.[1] This conservative approach detracts from the greatest benefit of metamaterials, viz. their ultralight weight.

Low-density metamaterials have evolved from honeycomb sandwich boards[4] and disordered foams[5] to highly complex topologies across a variety of size scales and base materials.[1] The rapid advances in the use and design of metamaterial have resulted in the introduction of new topologies to the scientific community, outpacing understanding on the deformation mechanisms of each new topology. Additionally, there is no consistency among studies in terms of base material, cell size, or AM process, which makes comparisons of various topologies across reported studies at best difficult and at worst speculative. Mechanical metamaterials are known to exhibit tension and compression asymmetry[6] as well as orientation-dependent anisotropic behavior when loading due to the lack of rotational symmetry of many topologies.[7] Additional studies on metamaterials have found the shear strength of metamaterials to be significantly lower than their uniaxial strength.[8] Because of this, metamaterials have a

(Received October 5, 2021; accepted November 5, 2021; published online November 29, 2021)

complex, nontrivial yield envelope that is crucial for engineers to understand to design metamaterial components with confidence.

The goal of the current study is to determine the effect of topology, particularly stretching- and bending-dominated topologies, on the size and shape of the yield surface. The Mohr–Coulomb failure criterion is chosen for this study as it can account for tension–compression anisotropy, and the failure envelope can be determined by using three tests: tension, compression, and pure shear.[9]

METHODS AND MATERIALS

Four cellular metamaterial topologies of interest were produced by AM via fused deposition modeling: a traditional honeycomb, an auxetic honeycomb, a triangular, and a circular topology. Topologies were modeled using a 5-mm unit cell and 0.6 mm wall thickness and were printed using a Dremel 3D45 printer with Dremel Eco-ABS white filament.[10] Each topology was tested in two orientations, denoted as direction 1 and direction 2, where direction 2 is a 90° in-plane rotation of direction 1 (Fig. 1).

Specimens of all four topologies were tested in tension, compression, and shear to populate Mohr's circle. Three specimens of each type were tested in each loading condition, and the yield strengths calculated by a 0.02% offset were averaged. As the specimens yielded, the stress–strain curves showed a distinctly sharp change in slope at yield. To consistently report the yield strength as indicated by the sharp change in slope, a 0.02% offset was used rather than the more traditional 0.2% offset.

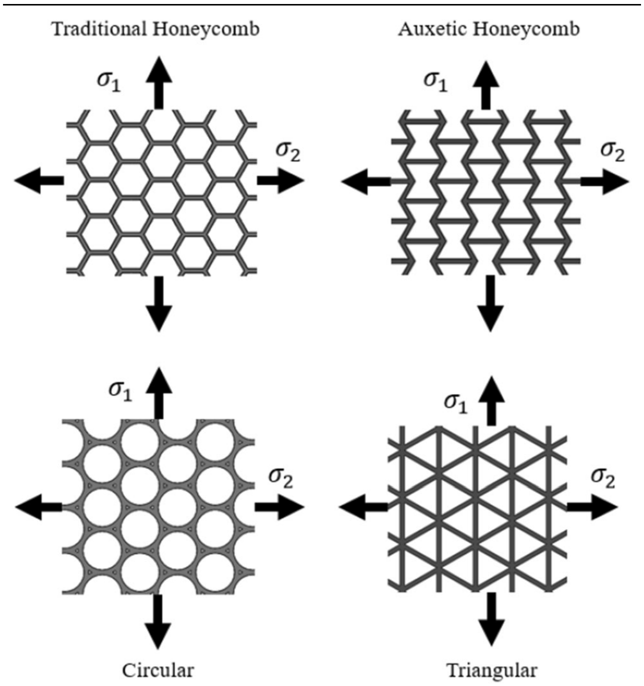

Fig. 1. Cellular material topologies tested with original orientation (σ_1) and 90° rotation (σ_2).

This approach is adopted from Ref. 11 which first addressed the issue of strain hardening in some topologies while reporting the yield of metamaterials.

Novel pure in-plane shear grips previously designed by the authors were used to ensure pure shear during the shear experiments rather than a combined shear and uniaxial loading state.[8] To validate the calculated yield surfaces, the honeycomb and triangle specimens were modified for mixed loading and two specimens were tested for various mixed loading profiles, and the averaged results plotted on the yield surface.

Uniaxial and shear experiments were performed under displacement control at a rate of 30 μm/s using a hydraulic load frame for the shear specimens and a screw-driven load frame for the tension and compression samples. Mixed shear–tension and shear–compression loading experiments were performed using a custom-made screw-driven biaxial load frame at the Pennsylvania State University Behrend campus. Custom shear grips were made for the shear tests, with a sliding base that prevented an induced tensile load from being applied to the specimen. Previous work identified induced tensile loads as artificially revealing a higher shear strength in metamaterials.[8] Traditional torsional experiments to measure shear behavior could not be used to measure in-plane shear strength, necessitating the custom grips. A custom mixed loading grip was also designed, with two sliding bases to prevent a horizontal induced tensile load and to keep the specimen centered during loading. The mixed loading test setup is shown in Fig. 2.

Digital image correlation was used to measure local and global displacements of the specimen throughout the experiment and calculate the corresponding strain fields. A single camera captured a 6 $\times$ 4 unit cell cross-section of the center of each specimen during tests. The camera used was a Point Grey model GS3 equipped with a Navitar lens and a 0.5$\times$ adaptor, capturing images at a rate of 1 Hz. Images were used to calculate the full-field displacement and strains using commercial digital image correlation software (VIC 2D). Strain calculations were performed using a virtual strain gage of 21 pixels^2 and a spatial resolution of 35 pixels^2 following the procedure outlined in Ref. 12. Global material properties were calculated using the area methodology outlined in Ref. 7.

RESULTS

Yield Surfaces

Experimentally determined tension, compression, and shear yield stresses for each orientation of the chosen topologies were plotted on Mohr's circle, shown for the honeycomb topology in Fig. 3a and b. The maximum shear line was calculated by plotting a linear line between the maximum shear value of each Mohr's circle. The maximum shear line is

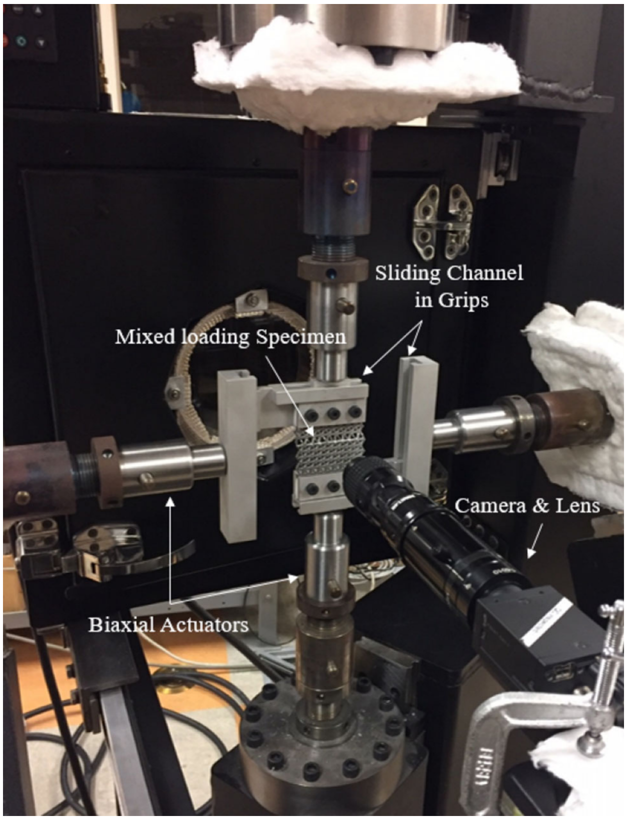

Fig. 2. Validation experimental setup in biaxial load frame. Grip is designed with two sliding bases to enable deformation in shear while keeping the specimen centered during loading.

shown in green in Fig. 3a and b. Although this calculated line crossed through the tension and compression experiment Mohr's circles, it results in a preferred, conservative yield envelope. As cellular materials are sensitive to defects resulting from the AM process, a conservative yield criterion is preferable. Using the Mohr's circles, an in-plane yield surface was created for each topology and is shown overlaid in Fig. 3c.[9] The two yield surfaces collapsed to one surface for the material using all six experimentally determined yield strengths to create a surface, showing full tension–compression–shear anisotropy as well as the orientation-specific anisotropy (Fig. 3d). The yield surfaces for each orientation are shown in Fig. 4, where the top row shows the yield surface for each orientation, the middle row the combined yield surface, and the bottom row an image of the corresponding topology.

The decreased shear strength of these cellular materials resulted in a discontinuity at the pure shear loading condition. The metamaterial was weaker in shear than would be expected from the maximum-distortion-energy theory or the more conservative maximum-shear-stress theory.[13] This behavior was seen for each topology.

Topology Effects

The stretching-dominated triangle topology had the largest yield surface with maximum tensile, compressive, and shear strength of 21.1 MPa, – 28 MPa, and 12 MPa, respectively, compared with the honeycomb topology, which had the second largest yield surface, with maximum tension, compressive, and shear strength of 12 MPa, – 11.9 MPa, and 7.4 MPa, respectively (Fig. 5a). The triangle topology is plotted on a different scale than the other topologies in Fig. 4 due to its greater strength. The increased strength of stretching- over bending-dominated topologies has been well documented in metamaterials research.[14–17] When bending-dominated topologies are strained, the struts rotate (Fig. 5c and d), increasing the angles between struts, which results in localized plastic deformation and buckling of a single strut (circled in red in Fig. 5c), corresponding to the global yield of the specimen. Figure 5c and d were taken after yield to illustrate the buckling cell wall. When a stretching-dominated topology such as the triangle is strained, the struts do not rotate as the bending topologies do; rather, there is just a high concentration of strains highly localized at the strut junctions, even at low global displacements.[16] These strains in the triangle topology are circled in red in Fig. 5b, taken at 0.5 σ_{yield}.

The increased strength of the honeycomb topology in comparison with other bending-dominated topologies is due to the uniform deformation of the honeycomb unit cells. As the honeycomb is deformed, plastic hinges form as the arms rotate, absorbing energy and increasing the toughness as circled in red in Fig. 6a. Uniform deformation allows the plastic hinges to develop without the stress concentration at any one plastic hinge becoming so large that the metamaterial fractures prematurely.[7] Fig. 6 is shown after yielding to better illuminate the locations of strain and plastic hinges within the topologies, but the onset of crazing at plastic hinges has been shown to occur prior to yielding.[7,18] The circle topology does not have sharp corners for plastic hinges to form. Additionally, the hourglass shape of each strut creates a local stress concentration in the middle, identified by the high strain circled in red in Fig. 6b. The local stress concentration leads to early fracture of individual struts, thus lowering the yield stress as the specimen yields globally when the first strut fractures, creating a smaller yield surface than the honeycomb topology. The auxetic honeycomb also develops plastic hinges when loaded; however, the auxetic honeycomb has a negative Poison's ratio.[19] As the auxetic honeycomb is loaded in tension, the horizontal struts are loaded in compression due to the negative Poison's ratio (the struts in the honeycomb topology are loaded in tension). The auxetic unit cells rotate when loaded to decrease the compressive stress on the horizontal strut, changing the loading path and nonuniformly

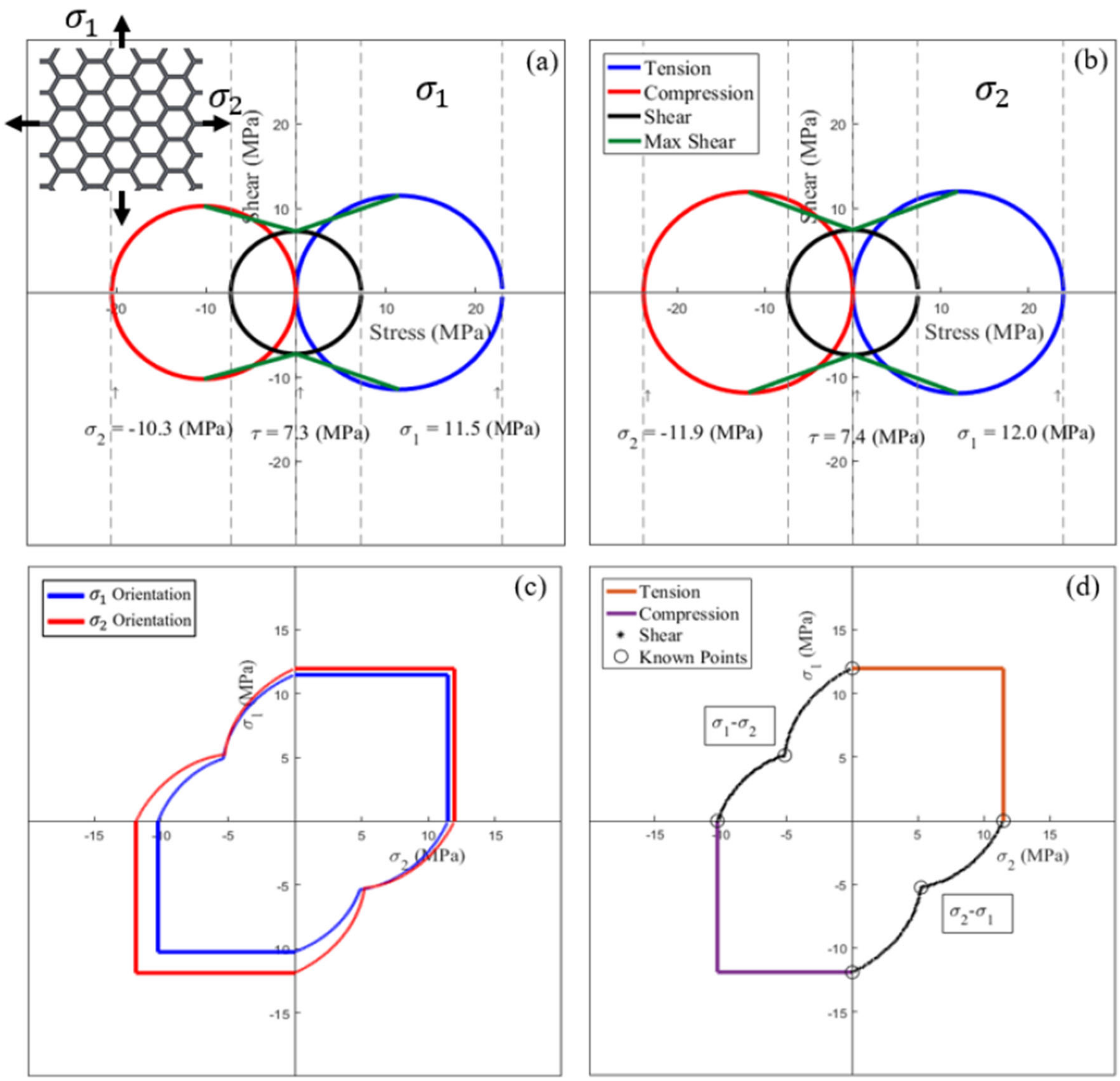

Fig. 3. Honeycomb Mohr's circle in (a) σ_1 and (b) σ_2 loading directions, (c) overlay of the σ_1 and σ_2 yield surfaces and (d) calculated full in-plane yield surface of combined σ_1 and σ_2 loading.

increasing the stress concentrations at the plastic hinges. The auxetic specimen yields when the plastic hinges with the largest strain concentrations (such as that circled in Fig. 6c) fracture.

The triangle topology had the largest 1–2 orientation anisotropy, with an 80% difference in tensile strength and 66% difference in compressive strength, with the 2-direction showing higher strength than the 1-direction in both loading conditions. When the triangle topology is loaded in the 1-direction, the axial load is primarily distributed among a third of the struts, i.e., those parallel to the loading direction. The positive axial load path is marked in red in Fig. 7a and supported by the concentration of positive strains along these struts shown in Fig. 7c. When loaded in the 2-direction, the axial load is distributed among the angled struts (Fig. 7b), consisting of two-thirds of the struts in the topology, as demonstrated by the positive strains in Fig. 7d. This difference in load distribution between the 1- and 2-orientations explains why the tension and compression yield strength of the 2-direction are nearly twice the values for the 1-direction.

Yield Surface Validation

Mixed loading validation tests were performed for the honeycomb and triangular topologies to compare the calculated yield surface with experimental results of the complex loading regions of the surface. The triangle and honeycomb topologies were chosen to represent a stretching- and a bending-dominated topology. The mixed loading specimens were subjected to combined tension–shear or compression–shear loading. The applied shear and uniaxial loads were combined to calculate the effective stress and the in-plane principal stresses following Eqs. 1 and 2 The effective strain was calculated using the local strains calculated via digital image correlation via Eq. (3).

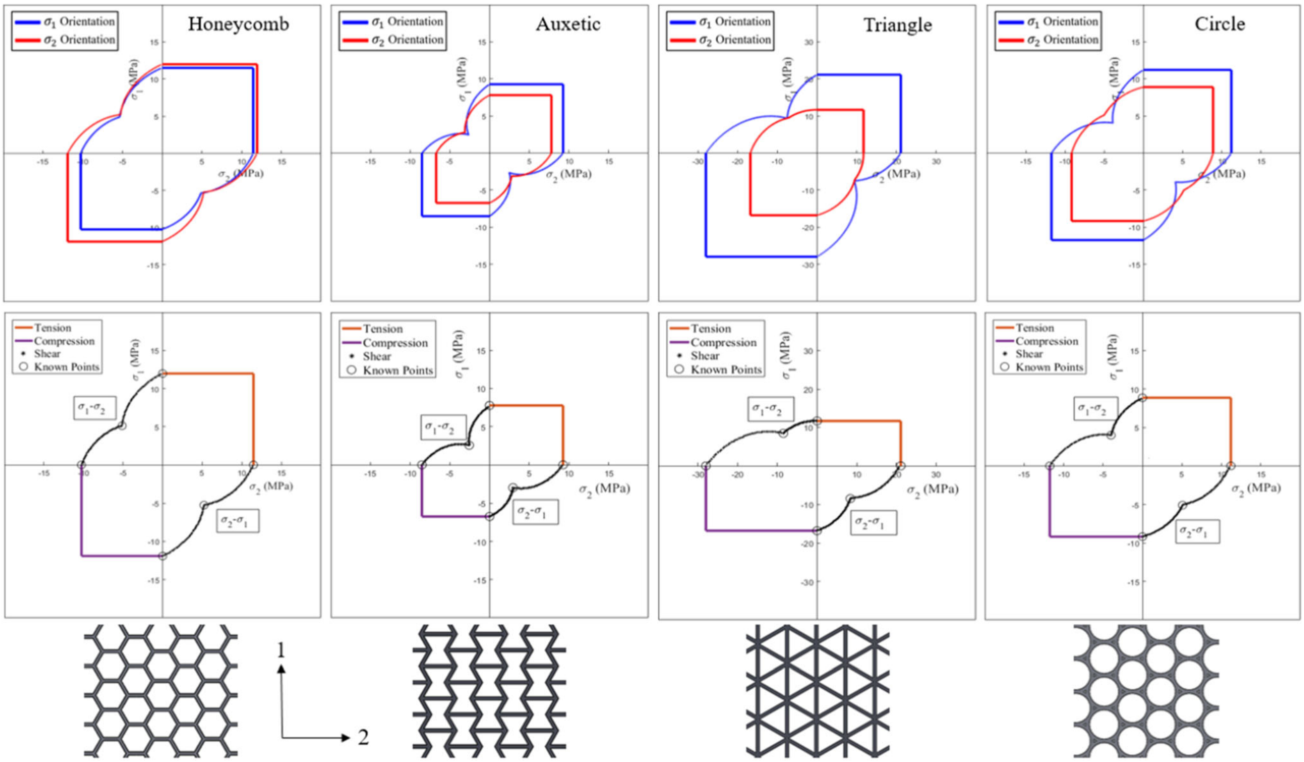

Fig. 4. Yield surface for the four topologies. Top row: yield surface for each orientation. Middle row: full-field surface for topology. Bottom row: selected topology. Note: Scale adjusted for the triangle orientation.

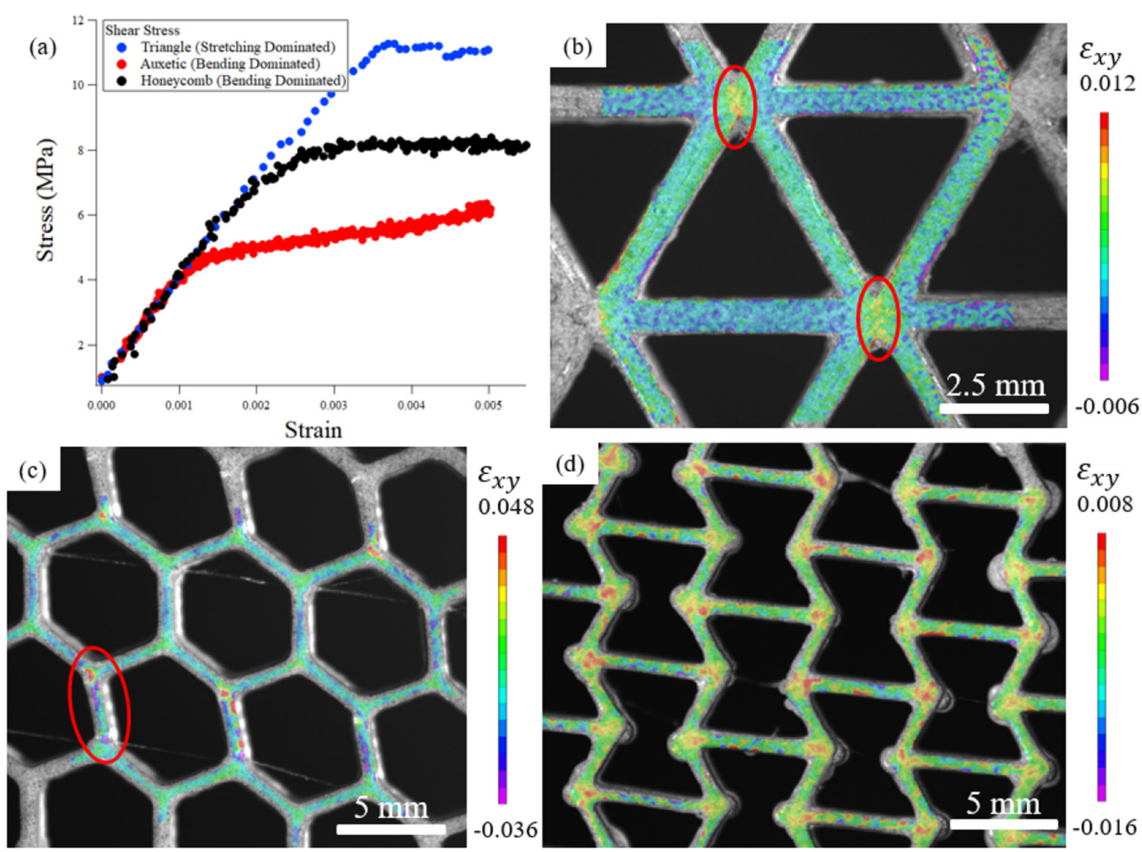

Fig. 5. (a) Shear stress–strain curves of selected topologies. (b) Strain maps of triangle in shear. (c) Strain maps of honeycomb in shear. (d) Strain map of auxetic in shear.

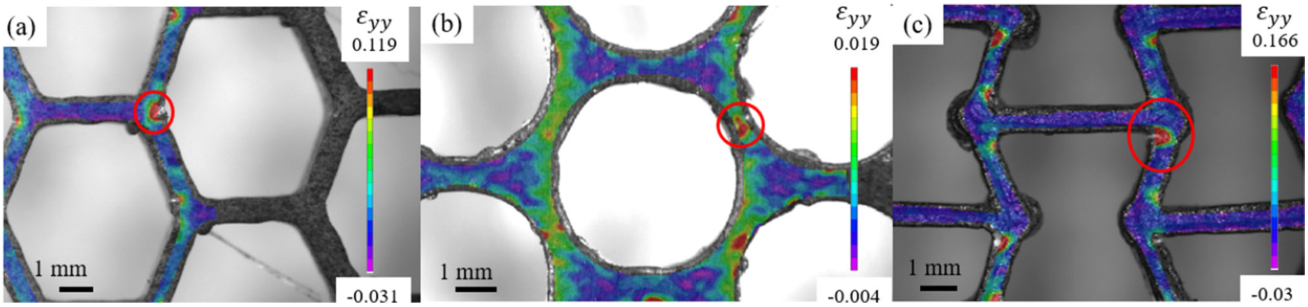

Fig. 6. Strain maps of bending-dominated topologies, (a) honeycomb, (b) circle, and (c) auxetic, in σ_1 orientation under tensile loading (all figures at the same scale).

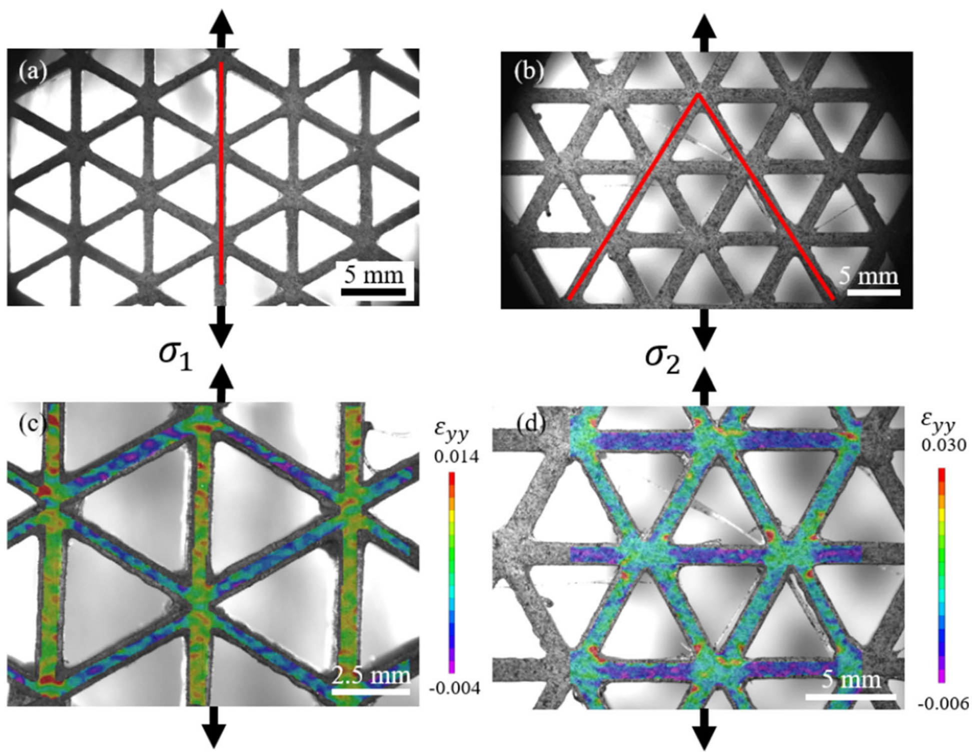

Fig. 7. Loading path for the triangle topology in the (a) σ_1 and (b) σ_2 orientations where (c) and (d) local tensile strain concentrated along indicated struts.

$$\sigma_{\text{eff}} = \sqrt{\frac{3}{2}\left[\sigma_x^2 + \sigma_y^2 + 2\tau_{xy}^2\right]} \tag{1}$$

$$\sigma_{1,2} = \frac{\sigma_x + \sigma_y}{2} \pm \sqrt{\left(\frac{\sigma_x - \sigma_y}{2}\right)^2 + \tau_{xy}^2} \tag{2}$$

$$\varepsilon_{\text{eff}} = \frac{2}{3}\sqrt{\frac{3}{2}\left(e_{xx}^2 + e_{yy}^2\right) + \frac{3}{4}\left(\gamma_{xy}^2\right)} \tag{3}$$

Using the 0.02% offset method discussed above, the effective yield stress was determined, then the principal stresses corresponding to the effective yield strain were plotted onto the yield surface. The mixed loading yield points are superimposed over the calculated yield surfaces in Fig. 8, with the yield points shown in blue. The validation experiments showed good agreement with the calculated surface, minimally underestimating the strength of the metamaterial. As the applied shear force was increased, with respect to the tensile or compressive load, the strength of the metamaterial decreased, following the curvature of the yield surface. The average strength of the mixed loading honeycomb specimen was 20.7% greater than that predicted by the yield surface, with the smallest difference being 7.2% and the largest difference 32.4%. The average strength of the mixed loading triangle specimen was 15.6% greater than that predicted by the yield surface, with the smallest difference being 1.1% and

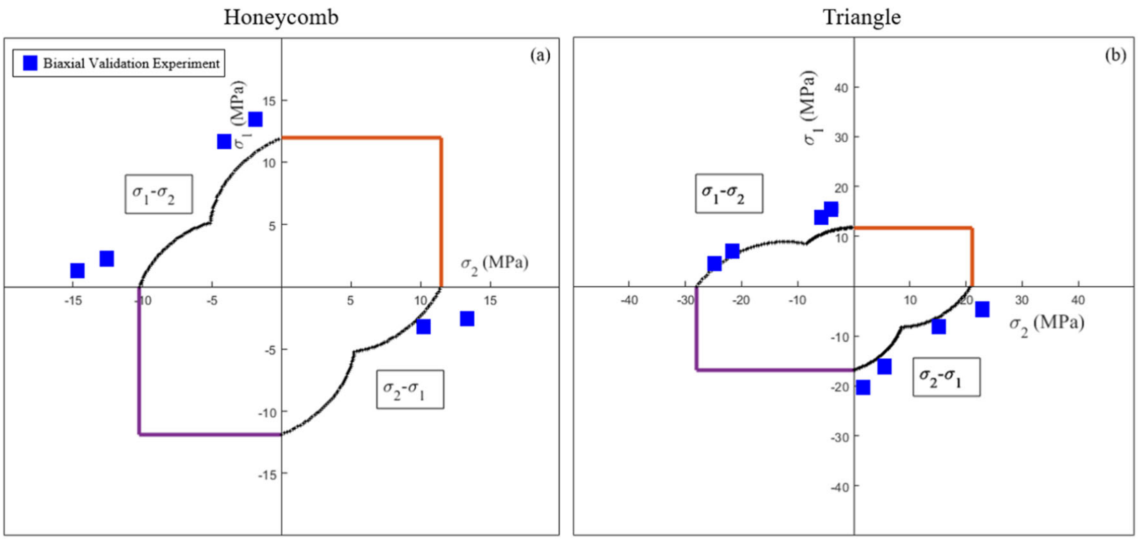

Fig. 8. Mixed shear–tension and shear–compression loading tests (blue squares) used to validate the (a) honeycomb and (b) triangle topology yield surfaces. Tests showed good agreement with the calculated surface, with the conservative tangential line slightly underpredicting the strength of the specimens.

the largest difference 26.6%. Even though the percentage strength differences appear large, the differences in magnitude are reasonable due to the small yield strengths of the cellular metamaterials.

DISCUSSION

Traditionally, yield surfaces have been calibrated based on material tests in tension and compression.[13] Therefore, the location of the largest disagreements between different calculated yield surfaces is generally at pure shear, the classic example being between the von Mises and Tresca yield surfaces.[13] Several yield surfaces have been developed for metamaterials recently, considering the role of topology[20,21] and the complex and varied local loading within a metamaterial.[11] The cited studies observed similarities to what was found in this study, such as large yield surface size variation between stretching- and bending-dominated topologies[11] and the shape of the yield surface changing with topology.[20,21] The above findings show that metamaterials are weak in shear compared with their uniaxial strength because of the formation of plastic hinges and strains nonuniformly distributed among the metamaterial's struts. To create a yield surface that is not calibrated to a metamaterial's diminutive shear strengths would result in plastic deformation and failure when, according to the yield surface, the metamaterial should be under reversible elastic loading. Tension–compression anisotropy and orientation anisotropy of metamaterials are more often discussed than uniaxial versus shear strength mismatches, thus to date the focus of metamaterial yield surfaces has been on capturing the first two anisotropies.[11,20,21] This important discovery of poor metamaterial shear strength necessitates that a metamaterial yield surface also be calibrated to the metamaterial's strength in pure shear.

Inaccurate predictions of shear states in yield surfaces is an issue that is not just limited to metamaterials, but also monolithic but complex materials including rolled sheet metals.[22] A methodology was introduced in Ref. 22 by adding an additional shear constraint while calibrating an anisotropic yield surface to increase the accuracy in the shear stress state region. Adopting this methodology for the mathematical description of a metamaterial yield surface could improve the ability to predict and understand metamaterial deformation. An issue discussed in Ref. 22 however, is that the addition of shear constraints overconstrains the model. An alternative solution is to use yield functions with more flexibility or use nonassociated rather than associated flow rules. Additionally, the yield surfaces calculated in this study have a convex discontinuity at the location of pure shear (Fig. 4). Due to this, the derived metamaterial yield surfaces already violate the normality rule and Druker's postulate for a stable material, despite the fact that several metamaterial topologies do exhibit strain hardening. Therefore, the behavior of metamaterials already confines the yield surfaces to nonassociated flow rules.

CONCLUSION

A yield surface was created for four cellular material topologies tested in tension, compression, and shear. The yield surfaces demonstrated that cellular materials were weakest in shear loading and have large anisotropies dependent on loading condition and orientation. Local strain fields were used to identify the mechanisms driving the deformation of different topologies and the driving effect of the unit cell deformation mechanism on global plastic properties. Buckling of cell walls and the formation of plastic hinges were the main mechanisms to cause yielding within the materials, but rotation of the cell walls due to its negative Poison's ratio caused the auxetic topology to have the smallest yield surface. Mixed loading validation tests of the calculated yield surfaces showed good agreement, validating this methodology as a way of creating metamaterial yield surfaces.

ACKNOWLEDGEMENTS

This work was supported in part by Student Pathways in Engineering and Computing for Transfer Success, NSF Grant 1834081, the Clemson University Creative Inquiry Program, and the Clemson Graduate Travel Grant Service.

CONFLICT OF INTEREST

On behalf of all authors, the corresponding author states that there are no conflicts of interest

REFERENCES

1. X. Yu, J. Zhou, H. Liang, Z. Jiang, and L. Wu, *Prog. Mater. Sci.* 94, 114 (2018).
2. J.U. Surjadi, L. Gao, H. Du, X. Li, X. Xiong, N.X. Fang, and Y. Lu, *Adv. Eng. Mater.* 21, 1. (2019).
3. O. Al-Ketan, and R.K. Abu Al-Rub, *Adv. Eng. Mater.* 21, 1. (2019).
4. A. Petras, M.P.F. Sutcliffe, and M.P.F.S.A. Petras, *Compos. Struct.* 44, 237. (1999).
5. C. Chen, A.M. Harte, and N.A. Fleck, *Int. J. Mech. Sci.* 43, 1483. (2001).
6. F. Brenne, T. Niendorf, and H.J. Maier, *J. Mater. Process. Technol.* 213, 1558. (2013).
7. K.M. Conway, and G.J. Pataky, *Mater. Today Commun.* 17, 144. (2018).
8. K.M. Conway, S.S. Kulkarni, B.A. Smith, G.J. Pataky, G.M. Mocko, and J.D. Summers, *Solid Free. Fabr. Proc. 30th Annu Int. Solid Free. Fabr. Symp.* 2019, 2296–2313. (2019).
9. T.K. Pellinen, S. Xiao, S. Carpenter, E. Masad, H. Di Benedetto, and R. Roque, *J. Assoc. Asph. Paving Technol.* 74, 347. (2005).
10. Dremel Digilab 3D45 Filam. EcoABS 1 (2021).
11. M. Alkhader, and M. Vural, *J. Mech. Phys. Solids* 57, 871. (2009).
12. P. Reu, *Exp. Tech.* 39, 1. (2015).
13. R. C. Hibbler, *Mechanics of Materials*, 8th edn. (Pearson Prentice Hall, Upper Saddle River, NJ, 2011).
14. P. Köhnen, C. Haase, J. Bültmann, S. Ziegler, J.H. Schleifenbaum, and W. Bleck, *Mater. Des.* 145, 205. (2018).
15. M. Leary, M. Mazur, H. Williams, E. Yang, A. Alghamdi, B. Lozanovski, X. Zhang, D. Shidid, L. Farahbod-sternahl, G. Witt, I. Kelbassa, P. Choong, M. Qian, and M. Brandt, *Mater. Des.* 157, 179. (2018).
16. T. Maconachie, M. Leary, B. Lozanovski, X. Zhang, M. Qian, O. Faruque, and M. Brandt, *Mater. Des.* 183, 1. (2019).
17. X. Chen, Q. Ji, J. Wei, H. Tan, J. Yu, P. Zhang, V. Laude, and M. Kadic, *Int. J. Mech. Sci.* 169, 1. (2020).
18. K.M. Conway, and G.J. Pataky, *Eng. Fract. Mech.* 211, 114. (2019).
19. Y. Sun, and N.M. Pugno, *Compos. Struct.* 106, 681. (2013).
20. B.B. Babamiri, B. Barnes, A. Soltani-Tehrani, N. Shamsaei, and K. Hazeli, *Addit. Manuf.* 46, 102143. (2021).
21. B. Bahrami Babamiri, H. Askari, and K. Hazeli, *Mater. Des.* 188, 108443. (2020).
22. A. Abedini, C. Butcher, T. Rahmaan, and M.J. Worswick, *Int. J. Solids Struct.* 151, 118. (2018).